Contact resistance study of noble metals and alloy films using a scanning probe microscope test station

L. Chen
Department of Electrical and Computer Engineering, Northeastern University, Boston, Massachusetts 02115, USA

H. Lee
School of Advanced Materials Engineering, Andong National University, Andong, Kyungbuk 760-749, South Korea

Z. J. Guo and N. E. McGruer[a)]
Department of Electrical and Computer Engineering, Northeastern University, Boston, Massachusetts 02115, USA

K. W. Gilbert and S. Mall
Department of Aeronautics and Astronautics, Air Force Institute of Technology, Wright-Patterson Air Force Base, Ohio 45433, USA

K. D. Leedy
Sensors Directorate, Air Force Research Laboratory, Wright-Patterson Air Force Base, Ohio 45433, USA

G. G. Adams
Department of Mechanical and Industrial Engineering, Northeastern University, Boston, Massachusetts 02115, USA

(Received 22 March 2007; accepted 7 August 2007; published online 8 October 2007)

The proper selection of electrical contact materials is one of the critical steps in designing a metal contact microelectromechanical system (MEMS) switch. Ideally, the contact should have both very low contact resistance and high wear resistance. Unfortunately this combination cannot be easily achieved with the contact materials currently used in macroswitches because the available contact force in microswitches is generally insufficient (less than 1 mN) to break through nonconductive surface layers. As a step in the materials selection process, three noble metals, platinum (Pt), rhodium (Rh), ruthenium (Ru), and their alloys with gold (Au) were deposited as thin films on silicon (Si) substrates. The contact resistances of these materials and their evolution with cycling were measured using a specially developed scanning probe microscope test station. These results were then compared to measurements of material hardness and resistivity. The initial contact resistances of the noble metals alloyed with Au are roughly proportional to their resistivities. Measurements of contact resistance during cycling of different metal films were made under a contact force of 200–250 μN in a room air environment. It was found that the contact resistance increases with cycling for alloy films with a low concentration of gold due to the buildup of contamination on the contact. However, for alloy films with a high gold content, the contact resistance increase due to contamination is insignificant up to 10^8 cycles. These observations suggest that Rh, Ru, and Pt and their gold alloys of low gold content are prone to contamination failure as contact materials in MEMS switches. © *2007 American Institute of Physics*.
[DOI: 10.1063/1.2785951]

I. INTRODUCTION

The demand for miniature devices with high performance in many technical fields is increasing. Microelectromechanical systems (MEMSs) can fulfill this need through production of miniature devices with low power consumption and high performance.[1–3] One such MEMS device, the metal contact MEMS switch, has received considerable attention for use in space-based radar, phase shifter circuits, tunable rf filters, etc.[4] This switch needs to have low contact resistance (i.e., less than 2–3 Ω) and high reliability (i.e., $\sim 10^{11}$ cycles) for optimal performance.[5] In order to meet these requirements, the selection of the electrical contact material and packaging are probably the most critical steps. The contact materials should have low resistivity for low contact resistance, high hardness for protection against surface degradation, and high resistance against chemical attack/corrosion. In the case of macroswitches, numerous contact materials have been tested and adapted for use over the last several decades. Among them, silver and its alloys have been very widely used. However, these materials tend to form nonconductive sulfide layers on the surface, which in turn prevents their use in MEMS switches because the contact force of a typical MEMS switch, unlike a macroswitch, is not high enough to break through the sulfide surface layer.[6]

[a)]Electronic mail: mcgruer@ece.neu.edu

TABLE I. Deposition power and rate for single metal and co-sputtered metal films. (Note: deposition rate for alloys is cumulative for both targets. Sputter power for alloys is noted as Au power/metal power.)

	Au	Pt	Rh	Ru	Au–30%Rh	Au–70%Rh	Au–5%Ru	Au–10%Ru	Au–20%Ru	Au–30%Ru	Au–70%Ru	Au–10%Pt	Au–50%Pt
Power (W)	250	250	250	250	250/254	47/250	250/56	250/103	250/197	168/250	33/250	250/54	127/250
Deposition rate (nm/min)	87	48	40	27	126	57	95	101	104	87	39	95	87

Therefore, there is a need to explore alternative contact materials for MEMS switches.

Gold contacts have been widely used in metal contact MEMS switch design.[7–9] Low hardness, high conductivity, and inertness to contamination make Au very suitable for low force applications. However, soft gold contacts have been observed to be susceptible to contact wear[10] and adhesive failure.[11] In order to overcome this problem, researchers are working on finding harder materials for better reliability performance. Schimkat[12] used a piezocontrolled contact testing system to evaluate contact materials (Au, Au–5%Ni, and Rh). He suggested that Au–5%Ni and Rh, with lower adherence forces than Au, may be better candidates for MEMS switch design. Majumder *et al.*[4] reported that a "platinum group" metal contact can be reliably cycled up to 10^{11} times under cold switching conditions. Coutu *et al.*[13] tested Au–6.3%Pt contacts up to 2.7×10^{8} cycles under "hot-switch" conditions. This set of works indicates that noble metals or Au alloys may be good candidate materials for contact MEMS switches.

To study contact materials for rf MEMS switches, we built a customized scanning probe microscope (SPM) test station and investigated the contact resistance of three noble metals (Pt, Rh, and Ru) and their alloys with Au. The thin films for contact tests were deposited using dc magnetron sputtering, and the hardness of the films was measured by instrumented nanoindentation.[14] The flexibility of the customized SPM test station allows us to tailor and measure the contact forces as well as the contact environment. We found that the evolution of contact characteristics during the cycling tests is closely related to reliability problems in real MEMS switch operation. Thus, the present study investigates the contact resistances of Pt, Ru, and Rh and their alloys with Au using this specially designed SPM-based setup. The contact resistance results are correlated with resistivity, hardness, and elastic modulus obtained from nanoindentation testing. The reliability performance of different contact materials is also evaluated by cycling contacts and monitoring the evolution of contact resistance. The buildup rate of contamination is indicated by the increase of contact resistance. Contact materials with different surface reactivities show distinctive contact resistance evolution characteristics. It is expected that these results may provide guidelines and improved understanding of electrical contact materials for rf MEMS switches.

II. EXPERIMENTS

Thin films having a nominal thickness of 300 nm were deposited on silicon substrates from 99.95% pure Au, Pt, Rh, and Ru in a Denton Vacuum Discovery 18 dc magnetron sputtering system with a base vacuum of 1.4×10^{-6} Pa. A mass-flow regulated argon (Ar) sputtering pressure of 0.32 Pa was used for all depositions except for Pt depositions at 1.06 Pa. Substrate materials were 75 mm diameter and 380 μm thick (100) silicon wafers. Substrates were cleaned in a buffered oxide etch solution, nitrogen dried and Ar plasma cleaned for 5 min at 60 W prior to deposition. Table I shows the alloys studied, deposition rates, and cathode powers used to achieve the alloy films. Further details of the thin film deposition procedure can be found in a previous report.[14]

Nanoindentation tests were conducted using a Nanoindenter XP (MTS system, Oak Ridge, TN) with a Berkovich tip using a dynamic contact module (DCM) which has displacement and load resolutions of 0.5 nm and 2 nN in air, respectively. A total of 15 indentations were conducted on each specimen using the continuous stiffness measurement (CSM) technique;[15] the average values of these 15 indentations are presented in the present study. More details of the nanoindentation measurement technique can be found in Ref. 14. Film resistivity was calculated from the sheet resistance measured by a standard four-point probe and the film thickness was measured using a profilometer. At least ten sheet resistance measurements were obtained across each of the thin film wafers to ensure uniform material deposition.

Contact characteristics were studied with a contact tester developed using a scanning probe microscope (JSPM-5200, JEOL, Tokyo, Japan). As shown in Fig. 1, the contact bumps are approximately 2.5 μm in diameter and 1 μm tall and were fabricated on top of a cantilever using a silicon micromachining process. The bumps were made by wet etching a 1 μm thick thermally grown silicon oxide layer using a buffered oxide etch solution. Contact was made using a piezoelectric actuator (PL022, Physik Instrumente, Auburn, MA) mounted on the SPM stage to press a flat substrate against the contact bump of the cantilever. The size of the silicon cantilevers is $80\times30\times180$ μm^3, with a spring constant of about 1.5×10^{4} N/m, which was estimated from the measured dimensions of the cantilever. A schematic of the ex-

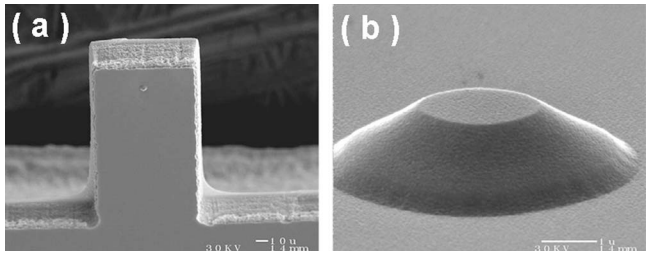

FIG. 1. SEM micrographs of (a) silicon cantilever and (b) contact bump on silicon cantilever.

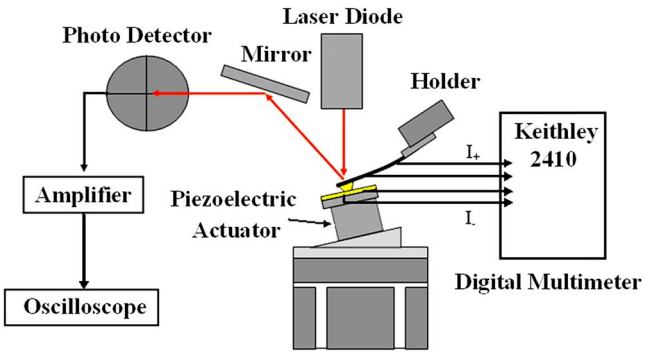

FIG. 2. Schematic of SPM-based setup for measuring contact resistance and contact force.

perimental apparatus is shown in Fig. 2. The contact force is proportional to the magnitude of the deflection, which is obtained from the optical system of the SPM and the spring constant of the test cantilevers. The contact force was controlled by the displacement of the piezoelectric actuator and monitored by the deflection of the cantilever. Using this setup, it was possible to obtain a contact force in the range of 200–250 μN with a resolution of 25 μN in each test. Contact tests were performed between contact pairs of the same deposited material. Contact resistance evolution characteristics were studied by cycling the contact in a cold switching mode (voltage is only placed across the contacts when the surfaces are in contact).

A source meter (Keithley Instruments2410, Cleveland, OH) was used for four-wire contact resistance measurements with a 1 mA current source and a 2.1 V compliance voltage. Figure 3 shows the structure layout for the four-wire resistance measurement. There are four probes—two probes are attached to the cantilever and the other two probes are attached to the substrate. On the cantilever side, two testing probes are placed at the end of the cantilever. The sheet resistance from the metal thin film on the cantilever will be inevitably included in the measurement. On the substrate side, a voltage probe and a current probe are located separately on two opposite sides of the substrate, as shown in the Fig. 3. The contact area is located near the edge of the third side. This arrangement of contact probe greatly reduces the sheet resistance component from the substrate. Contact resistance measurements were done on as-deposited materials ex-

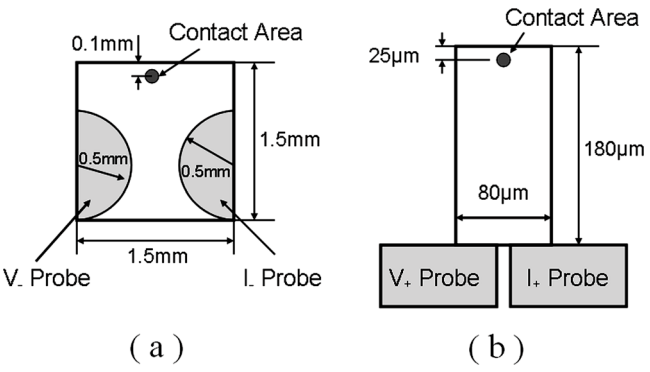

FIG. 3. Test layout for contact resistance measurement. (a) Substrate and (b) cantilever.

TABLE II. Hardness, modulus, and resistivity data of metal and metal alloys. [Note: the values were measured at 24 nm indentation for 300 nm thickness film using a Nanoindenter XP from MTS (Oak Ridge, TN).]

	Hardness (GPa)	Modulus (GPa)	Resistivity ($\mu\Omega$ cm)
Au	1.04	86	3.6
Pt	5.39	183	16.6
Rh	9.75	256	9.3
Ru	15.28	295	13.8
Au30%Rh	4.87	153	58.8
Au–70%Rh	9.57	217	44
Au–5%Ru	2.42	122	38.5
Au–10%Ru	3.99	137	56.5
Au–20%Ru	4.28	148	69.9
Au–30%Ru	6.18	154	87
Au–70%Ru	11.46	231	86
Au–10%Pt	2.79	124	15.2
Au–50%Pt	5.1	155	47.2

posed to ambient laboratory conditions for 72 h or more. Under these conditions, the contact was susceptible to contamination or formation of surface layers.

III. RESULTS AND DISCUSSION

Table II shows the hardness, elastic modulus, and resistivity of thin films of four metals (Pt, Rh, Ru, and Au) along with alloys between Au and the other three metals. The hardness values were taken at a 24 nm indentation depth (i.e., a depth of 8% of the film thickness). Compared to pure Au, the other noble metals have higher hardness and elastic modulus. By alloying the other noble metals with Au, both the hardness and elastic modulus are decreased. The reduction of the hardness and elastic modulus depends on the content of Au. The higher the content of Au, the lower the hardness and elastic modulus. At the same time, the resistivity of the alloys is significantly higher than that of the pure metals.

Figure 4 shows the relationship between the measured electrical resistivity and hardness as well as between the measured contact resistance (R_M) and hardness for metal and metal alloy films. Comparing Figs. 4(a) and 4(b), there are similar distribution patterns for the data of resistivity and the data of the measured contact resistance. The similarity between the resistivity and the measured contact resistance is because two major parts of the measured resistance are related to the resistivity of the material. One such part is the sheet resistance component (R_{SC}) from the resistance of the metal film on the cantilever and testing pads. This metal film resistance cannot be eliminated by the four-wire measurement because of practical limitations on contact placement. The other part of the measured contact resistance is from the constriction resistance (R_C) caused by the current flowing through a small contact area. For a force large enough to cause fully plastic deformation, the contact area is equal to the force divided by the hardness. The constriction resistance R_C for a single asperity contact between two half-spaces, with contact radius significantly larger than the mean free path for electrons, is given by[16]

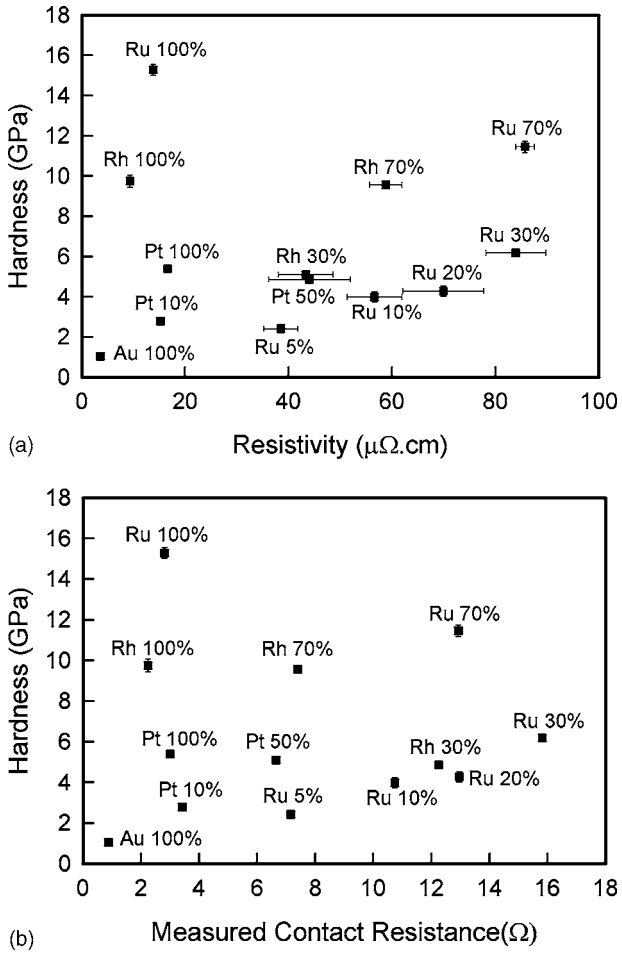

FIG. 4. Electrical resistivity (a) and measured contact resistance (b) for various thin films with hardness measured at a 24 nm indentation depth.

$$R_C = \frac{\rho}{2a}, \tag{1}$$

where ρ is the electrical resistivity and a is the radius of the contact spot (assumed to be circular). For a fixed value of the contact force, the constriction resistance should be proportional to the resistivity and vary with the square root of the hardness. Since both the constriction resistance and the resistance of the metal film are proportional to the electrical resistivity, the similarity in Figs. 4(a) and 4(b) is not surprising.

In addition to the constriction resistance (R_C) and the sheet resistance component (R_{SC}), our measured contact resistance (R_M) also includes a film resistance (R_F) from the contamination thin film between the metal contacts. In order to estimate the contribution of each component (R_C, R_{SC}, and R_F) to our measured contact resistance (R_M), a three-dimensional (3D) finite element model was built. The simulation was performed using the commercial finite element analysis (FEA) program ANSYS®, with the actual geometry, dimensions, and measured material properties. It is assumed that the contacts are single asperity contacts, and the contact area is plastically deformed to a circular region after loading. The contact radii are calculated by using the measured hardness and the applied loading force. The simulation performed with ANSYS® uses element Solid98, and the resistance values

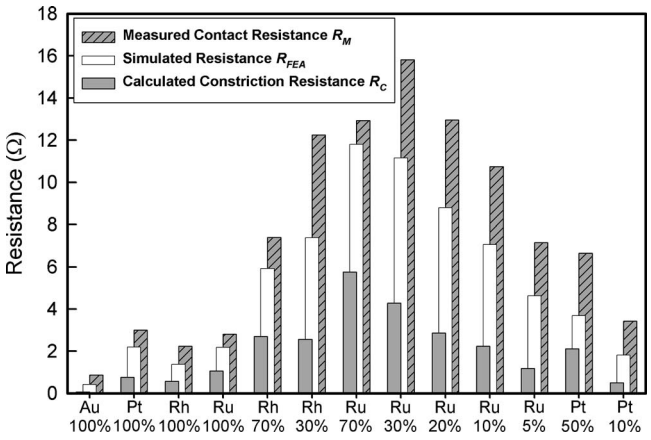

FIG. 5. Plot for measured contact resistance, simulated resistance, and calculated single asperity constriction resistance of metal and metal alloys.

of the cantilever and substrate are obtained by calculating the current through the conduction area for a given electrical potential. Let us denote the resistance value based on the finite element simulation as R_{FEA}. Note that the simulation results include both constriction and sheet resistance components ($R_{FEA}=R_C+R_{SC}$), but the contribution from contaminant films is not taken into account in the simulations.

Figure 5 shows the measured contact resistance (R_M), the calculated single asperity constriction resistance (R_C), and the simulation results (R_{FEA}) for the metals and alloys tested. The single asperity constriction resistance (R_C) was calculated from measured values of resistivity and hardness using Eq. (1). The difference between R_C and R_{FEA} gives the magnitude of the sheet resistance component from the cantilever and testing pads (R_{SC}). Our simulation results show that R_{SC} is typically one to two times as large as the constriction resistance R_C in our test structure.

The measured contact resistances (R_M) are 10%–100% larger than those estimated using the finite element model (R_{FEA}). This discrepancy between R_M and R_{FEA} may be due to either an overestimation of the contact radius or the existence of contamination films. To estimate the effect of the contact area on the resistance, we looked at the effect of varying the contact radius of Au–Au contact from the value of 247 nm, predicted from the measured hardness and applied force, to 50 nm. The total resistance predicted by ANSYS® (R_{FEA}) increased from 0.34 to 0.52 Ω. The predicted resistance is still much smaller than the measured value (R_M) of 0.85 Ω even when the contact radius is reduced to 50 nm. This indicates that errors in the size of the contact are not the dominant factor in this discrepancy. On the other hand, the effect due to contaminant films on resistance of metal contacts is known to be significant.[16,17] For instance, Holm[16] showed that the magnitude of resistance of contaminant films can be 2.3 times larger than the constriction resistance for Au–Au contact with a load of 1.15 g (~11.3 mN) at room temperature. Our measurements were performed when these thin films were exposed to ambient laboratory conditions for 72 h or more. Therefore, the difference between the measured resistance (R_M) and the simulated resistance (R_{FEA}) is probably largely due to the contamination film resistance (R_F).

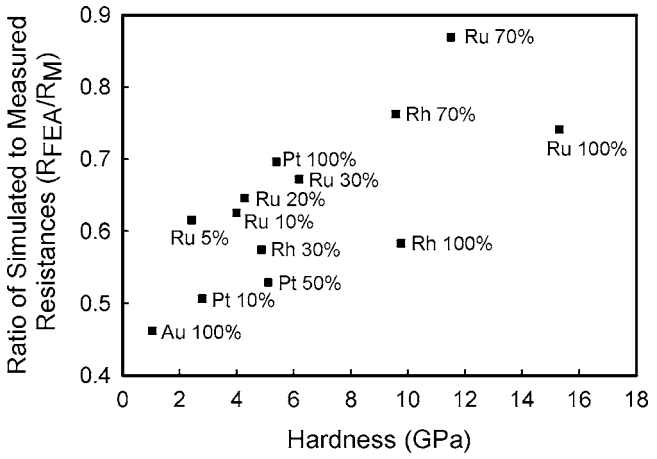

FIG. 6. The ratio of the simulated resistance to the measured contact resistance (R_{FEA}/R_M) for various thin films.

In addition, in Fig. 6, we plot the ratio of the ANSYS® simulated resistance to the measured total contact resistance (R_{FEA}/R_M) versus the hardness. The harder materials typically show a higher ratio of simulated to measured resistance values. Considering that the discrepancy between R_{FEA} and R_M is largely due to the film resistance (R_F), this observation may indicate that the surface films or contamination layers are less important in the harder materials. The harder material may more easily break or squeeze out the surface contaminant films than the softer materials. Furthermore, there will generally be more than one asperity contact in a metal contact. Harder materials are less likely to form single asperity contacts than the more easily deformable softer materials. Thus, the single asperity assumption may be less valid for the harder materials. For N asperities in contact, all plastically deforming, the average contact area will be the force divided by N times the hardness. The constriction resistance of the N asperities together will depend on the spatial distribution of the asperities, and will be bounded on the high end by the single asperity constriction resistance R_C and on the low end by the constriction resistance R_C^N, corresponding to all of the asperities conducting in parallel, i.e. Ref. 18,

$$R_C^N = R_C/\sqrt{N}. \tag{2}$$

For materials with more than one asperity in contact, the constriction resistance should be less than the value estimated by the single asperity assumption. Therefore, the single asperity model may overestimate the constriction resistance to a greater degree in the hard materials, leading to a higher ratio of the simulated value to the measured contact resistance in Fig. 6 for harder metals.

When contacts are cycled, buildup or wear-out of a surface film or contamination layer can strongly affect the measured contact resistances (R_M). Fig. 7 shows the measured contact resistance evolution characteristics of these materials in room air. The contact is susceptible to contamination and the contact resistances increase rapidly after a characteristic number of cycles for all materials tested except for gold, the Au–10%Pt and the Au–5%Ru alloy. This characteristic number of cycles of stable resistance increases from 10^4 for Ru to

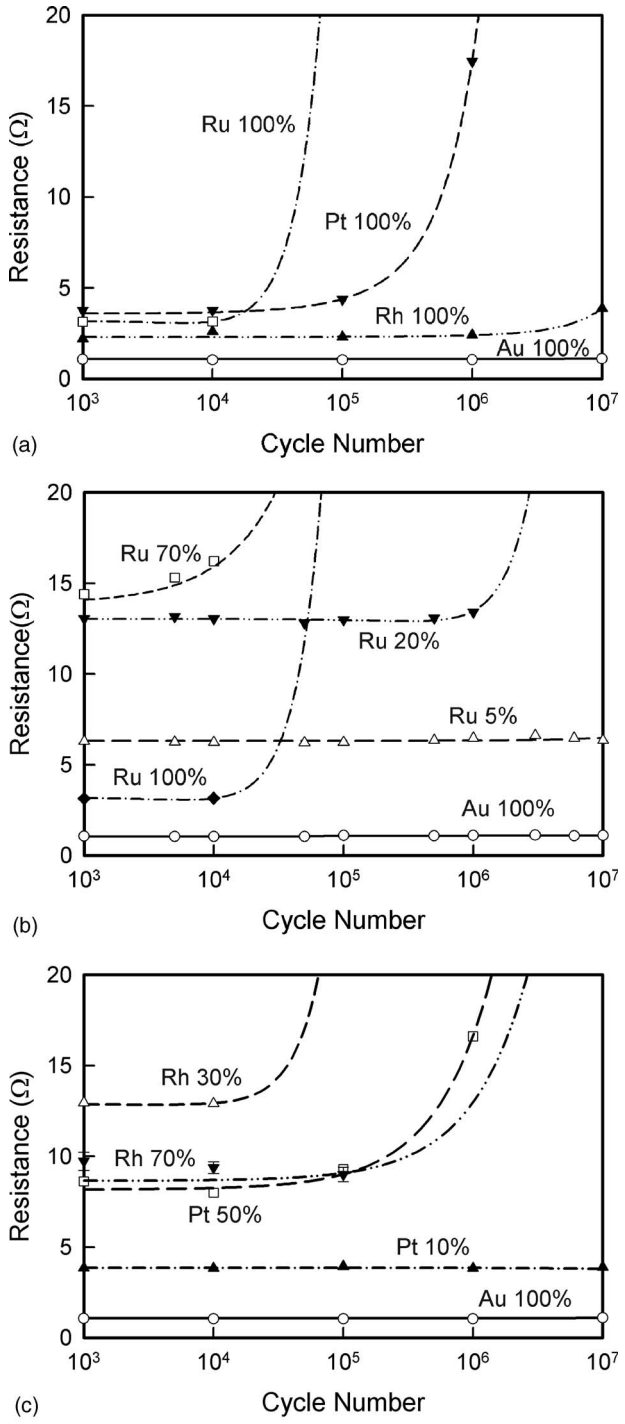

FIG. 7. Measured contact resistance (including constriction resistance, sheet resistance components, and film resistance components) evolution curves of (a) Ru, Pt, Rh, and Au; (b) Au and Au–Ru alloys; and (c) Au and Au alloys.

over 10^8 (not shown) for Au. Also, the characteristic number of cycles generally increases with an increasing percentage of gold in the alloy.

In pursuit of the cause of the increase of measured contact resistance, a scanning electron microscope (SEM) was used to inspect the contact surfaces after the cycling test. For contacts with increasing contact resistance, a layer of dark contaminant is observed around the bumps. Energy dispersive x-ray (EDX) analysis of this layer shows that the dark contaminants contain carbon (Fig. 8). They are suspected to

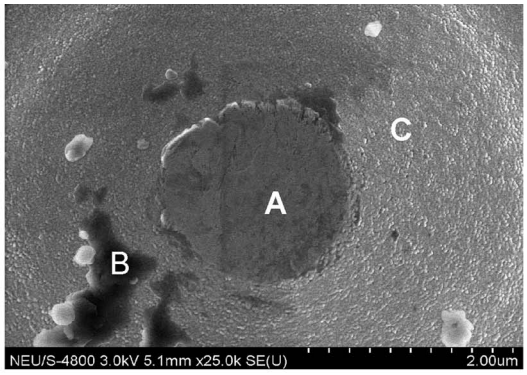

Element	Wt%	At%
C(K)	4.28	39.5
O(K)	0.65	4.51
Au(L)	94.35	53.14

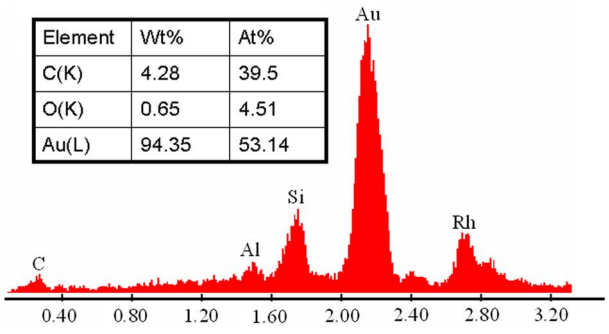

i) EDX spectrum at location A

Element	Wt%	At%
C(K)	8.01	58.83
O(K)	0	0
Au(L)	91.99	41.17

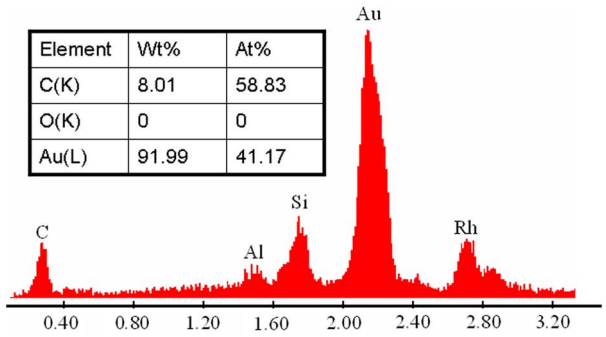

ii) EDX spectrum at location B

Element	Wt%	At%
C(K)	2.06	25.23
O(K)	0.17	1.61
Au(L)	97.77	73.17

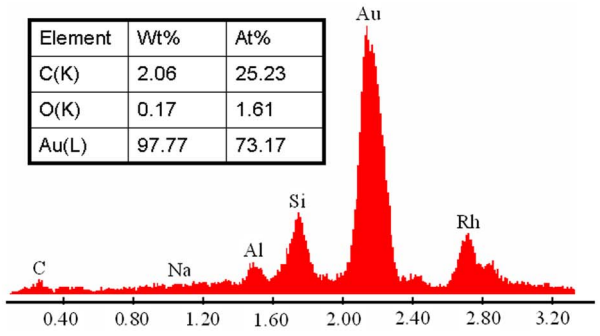

iii) EDX spectrum at location C

FIG. 8. SEM and EDX analysis of Au–30%Rh alloy contact surface after cycling test. (a) SEM micrograph; (b) EDX spectrum at three different locations on the bump: (i) top of bump, (ii) dark contaminant, and (iii) clean surface.

be frictional polymers.[19] Buildup of the frictional polymer increases the contact resistance rapidly. A high characteristic number of cycles before the resistance increase implies a lower rate of contamination buildup.

The different contamination rates for different metals and metal alloys could be related to their electron structure on the surfaces.[20,21] Ru, Rh, and Pt have partially filled *d*-band electron structures on the surface, which makes them likely to absorb molecules from the air and build up contaminant films. On the other hand, a filled *d*-band electron structure on the surface makes gold more inert to contamination. For metal alloys, the electron structure depends on the content of alloy elements. A first principles calculation[22] has shown that alloy elements can shift the *d*-band electron structure at the metal surfaces. It is not clear exactly how alloy elements change the electron structure of our test materials. However, we found that alloys with high Au content usually show lower contamination rates than those alloys with low Au content. This trend is clearly demonstrated in the Ru–Au alloy test [Fig. 7(b)]. By increasing the Au content in the alloy, the characteristic number of cycles with stable resistance increases from 10^4 for Au–70%Ru, to 10^6 for Au–20%Ru, and finally to more than 10^7 for the Au–5%Ru alloy. The contamination rate for Au–70%Ru is similar to that of Ru, while the contamination rate for Au–5%Ru is much lower.

Note that the increase of gold content can lower the hardness of Au alloys (Table II). Generally, contact materials with low hardness are more susceptible to contact wear. In order to investigate the effect of the alloy elements and its relation to wear rate and contamination rate, we compared the contact evolution properties of Au–5%Ru and Au–10%Ru. Both alloys were cycled for 10^6 cycles in room air followed by an inspection of the contact bumps with an SEM. After the cycling test, neither sample showed a large increase of contact resistance. The SEM micrographs for both bumps are shown in Fig. 9. The SEM image of Au–10%Ru shows a black contamination layer grown around the contact area, which is not observed in the Au–5%Ru sample. This indicates that the alloy with a higher percentage of gold is less prone to contamination failure. We also notice that there is contact wear on both contact surfaces. For Au–10%Ru, the fracture surface shows more brittle fracture characteristics. However, on the Au–5%Ru surface, there are small bright sharply raised areas in the SEM image which are characteristic of ductile fracture. This behavior may be due to the fact that Au–5%Ru has a lower hardness than Au–10%Ru, which makes Au–5%Ru more susceptible to ductile fracture.

Reliability problems will be different for different contact materials. Au contacts are observed to exhibit a changing pull-off force and contact damage during cycling tests. The changing pull-off force may lead to contacts permanently sticking together in real switch operation. In our test, the pull-off force for gold contacts has been observed to vary from 100 to 200 μN during cycling tests. However, for materials with higher hardness, the extent of contact wear and contact adhesion are greatly reduced. After cycling tests, only minor contact wear has been observed in Au–5%Ru, Au–10%Ru, Au–10%Pt, and Rh, as compared with Au, with detected maximum pull-off force of 50, 50, 75, and 50 μN, respectively. The reduction of the pull-off force in noble metals and their alloys, compared to a gold contact, may be due

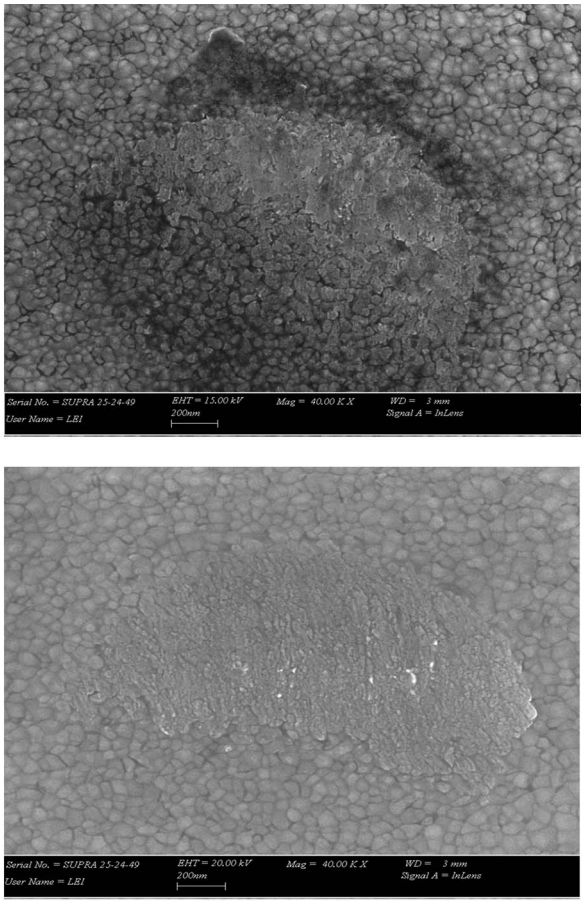

FIG. 9. SEM micrograph of Au–Ru alloy contact surface after 10^6 cycles test. (a) Au–10%Ru bump surface and (b) Au–5%Ru bump surface.

to the greater hardness and/or greater surface reactivity. When materials are subjected to the same contact force, the harder materials have smaller contact radii and smaller contact adhesion, which in turn leads to a lesser pull-off force to separate. In addition, the growth of the frictional polymer can further reduce the contact adhesion. After 10^5 contact cycles, the pull-off force typically decreases to less than our detection threshold of 25 μN for all contact materials tested with the exception of gold. Precautions such as surface deactivation treatment[23] and hermetic packaging for MEMS switches[4] are known to be at least partially effective in mitigating the effects of contamination. For many materials, contact failure may depend on the competition between two failure mechanisms—contact wear and contact contamination.

IV. CONCLUSIONS

Thin films of Pt, Rh, and Ru and their alloys with Au were deposited on silicon substrates and investigated as electrical contact materials for rf MEMS switches. The contact resistance was measured by a scanning probe microscope test station and related to measured values of material hardness and resistivity. The results show an increase in contact resistance and a decrease in hardness of Pt, Rh, and Ru by alloying with Au, and this increase/decrease was directly dependent upon the amount of Au. The overall trends in electrical resistivity and contact resistance with alloying were similar.

The contact resistance includes constriction, sheet, and film resistances. The initial contact resistance is greater than that predicted from the properties of the materials, probably because of contaminant films. The contact resistance prediction is closer to the experimental result for harder materials. This may indicate that contaminant films have relatively less influence on contact resistance for hard materials, or that there are more asperities in contact for those materials. However, surface films grow and greatly increase the contact resistance during cyclic operation. Compared with Au, the noble metals Ru, Rh, and Pt are more susceptible to the growth of a contamination film. When these metals are alloyed with Au, the alloying changes the contamination rate. High Au content in an alloy can make the metal less susceptible to contamination failure. These interrelationships among the contact resistance, hardness, and resistivity, along with the methodology used in the present study, help us to provide a basis for selection of optimum electrical contact materials for rf MEMS switches.

ACKNOWLEDGMENT

The views expressed in this article are those of the authors and do not reflect the official policy or position of the United States Air Force, Department of Defense, or the U.S. Government.

[1] J. J. Yao, J. Micromech. Microeng. **10**, R9 (2000).
[2] G. M. Rebeiz, *RF MEMS Theory, Design and Technology* (Wiley, London, 2003).
[3] V. K. Varadan, K. J. Vinoy, and K. A. Jose, *RF MEMS and their Applications* (Wiley, London, 2003).
[4] S. Majumder, J. Lampen, R. Morrison, and J. Maciel, IEEE Instrum. Meas. Mag. **6**, 12 (2003).
[5] G. M. Rebeiz, J. B. Muldavin, IEEE Microw. Mag. **12**, 59 (2001).
[6] H. E. Boyer and T. L. Gall T L, *Metals Handbook* (ASM International, Materials Park, OH, 1990), Vol. 2.
[7] S. Majumder, N. E. McGruer, and P. M. Zavracky, J. Vac. Sci. Technol. A **15**, 1246 (1997).
[8] E. J. J. Kruglick and K. S. J. Pister, J. Microelectromech. Syst. **8**, 264 (1999).
[9] J. Oberhammer and G. Stemme, J. Microelectromech. Syst. **15**, 1235 (2006).
[10] S. T. Patton and J. S. Zabinski, Tribol. Lett. **18**, 215 (2005).
[11] L. L. Mercado, S. M. Koo, T. Y. T. Lee, and L. Liu, *Proceedings of the IEEE Electronic Components and Technology Conference 2003*, New Orleans, LA, 2003, p. 377.
[12] J. Schimkat, Sens. Actuators, A **A73**, 138 (1999).
[13] R. A. Coutu, Jr., P. E. Kladitis, K. D. Leedy, and R. L. Crane, J. Micromech. Microeng. **14**, 1157 (2004).
[14] H. Lee, R. A. Coutu, Jr., S. Mall, and K. D. Leedy, J. Micromech. Microeng. **16**, 557 (2006).
[15] W. C. Oliver and G. M. Pharr, J. Mater. Res. **19**, 3 (2004).
[16] R. Holm, *Electric Contact*, 4th ed. (Springer-Verlag, Berlin, 1967).
[17] J. W. Tringe, T. A. Uhlman, A. C. Oloiver, and J. E. Houston, J. Appl. Phys. **93**, 4661 (2003).
[18] S. Majumder, N. E. McGruer, G. G. Adams, P. M. Zavracky, R. H. Morrison, and J. Krim, Sens. Actuators, A **A93**, 19 (2001).
[19] M. Amtler, IEEE Trans. Compon., Hybrids, Manuf. Technol. **CHMT-8**, 87 (1985).
[20] B. Hammer and J. K. Norskov, Nature (London) **376**, 238 (1995).
[21] B. Hammer and J. K. Norskov, Surf. Sci. **343**, 211 (1995).
[22] J. Greeley and J. K. Norskov, Surf. Sci. **592**, 104 (2005).
[23] T. Yokokawa, T. Yano, C. Kawakita, K. Hinohara, A. Nagai, and T. Kobayashi, IEEE Trans. Compon., Hybrids, Manuf. Technol. **CHMT-10**, 42 (1987).